NUCLEAR SCIENCE AND ENGINEERING: **12**, 169–177 (1962)

Neutron Capture to Fission Ratios in U^{233}, U^{235}, Pu^{239}*

J. C. HOPKINS AND B. C. DIVEN

Los Alamos Scientific Laboratory, University of California, Los Alamos, N. M.

Received April 17, 1961

The ratio of neutron capture to fission cross sections, α, has been measured for U^{233}, U^{235}, and Pu^{239} at 9 incident neutron energies from 30 kev to 1000 kev. A pulsed and collimated neutron beam is passed through a target placed at the center of a large, cadmium-loaded, liquid scintillator. Capture and fission events are detected by means of their prompt gamma rays; elastic and inelastic scattering events are discarded because of their smaller pulse height. Fission is identified by the delayed pulses produced by capture in the scintillator of the fission neutrons. Corrections are applied for the fission events not followed by delayed neutron pulses and for the effect of background counts. This procedure yields values of $1 + \alpha$ to an accuracy of 1 or 2%.

NOMENCLATURE

B_0 fraction of 32-μsec gates that do not contain one or more background pulses

C_0 fraction of 32-μsec gates, triggered by a fission event, that do not contain one or more fission neutron pulses

α ratio of neutron capture cross section to neutron-induced fission cross section

η the number of neutrons per fission available for fission and breeding, $\eta = \bar{\nu}/(1 + \alpha)$

$\bar{\nu}$ average number of neutrons emitted per fission

σ_c radiative neutron capture cross section

INTRODUCTION

A measurement of the ratio of neutron capture to neutron-induced fission cross sections, α, has been made for U^{233}, U^{235}, and Pu^{239}. This ratio has been measured at 9 incident neutron energies from 30 kev to 1000 kev. The neutron capture to fission ratio is of particular importance in the design of breeder reactors (*1*). The average number of fission neutrons per absorbed neutron is given by the quantity $\eta = \bar{\nu}/(1 + \alpha)$, where $\bar{\nu}$ is the average number of neutrons emitted per fission. Thus α is a measure of the rate at which reactor fuel is wasted by neutron capture.

The present measurement of α involves the detection of gamma radiation accompanying neutron capture and fission. A pulsed beam of neutrons from the T(p, n)He^3, or the Li^7(p, n)Be^7, reaction is allowed to strike a target placed at the center of a large liquid scintillator. Three processes can be initiated by the neutrons interacting with the target nuclei: neutron scattering, radiative capture, and fission. Both radiative capture and fission are accompanied by gamma-ray emission in coincidence with the beam pulse. This radiation is detected with almost 100% efficiency by the large liquid scintillator and produces a prompt pulse.

Fission, however, is also accompanied by neutron emission. This fact provides the basis for the technique used in this experiment, for distinguishing fission from capture events (*2*). The scintillator is large enough to cause most of the fission neutrons to be thermalized and finally captured in the liquid. The solution is cadmium loaded to ensure that approximately 95% of the neutrons will be captured within 32 μsec. The 9-Mev pulse produced by neutron capture in the cadmium provides delayed pulses to identify fission events.

The only interaction other than capture and fission produced in the target by neutrons of energy less than 1 Mev is scattering. Elastic scattering of a neutron by a target nucleus produces a delayed pulse in the scintillator but provides only a small prompt pulse produced by recoil protons during the slowing down of the neutron in the solution. Inelastic scattering can produce scintillator pulses, due to gamma radiation or recoil protons, but the sum remains less than about 1 Mev. Thus if we require that the prompt pulse correspond to more than 1 Mev of gamma radiation, all scattering events will be ignored.

If we neglect background corrections and the fact that not all fission events are followed by delayed pulses, the experiment is very simple. The prompt pulse is used as a trigger to open a delayed 32-μsec

* Work performed under the auspices of the U. S. Atomic Energy Commission.

gate between the scintillator and a pulse detector. If any pulses occur during the gate, the prompt pulse was caused by a fission event. However, if no pulses occur during the gate, the prompt pulse was due to radiative capture. The ratio of the number of capture to the number of fission pulses is α.

The corrections for the background radiation and the fact that not all fissions are accompanied by delayed pulses in the scintillator are discussed below.

EXPERIMENTAL PROCEDURE

The proton beam from a 2.5-Mev electrostatic accelerator is pulsed. The duration of a pulse is about 0.06 μsec and the pulses are separated by either 8 or 32 μsec. The peak current is about 100 μa. The average beam current is about 0.2 μa (for a 32-μsec pulse separation). Nearly all of the data were taken with a pulse separation of 32 μsec. It is necessary to have a pulsed neutron beam to discriminate against delayed pulses from scattered neutrons. Neutrons were produced by the $T(p, n)He^3$ and the $Li^7(p, n)Be^7$ reactions, both of which are endoergic. Two neutron groups are produced by monoenergetic protons for proton energies from the reaction threshold energy up to a laboratory energy of $E_p = -Qm_R(m_R - m_p)^{-1}$, where m_R is the mass of the residual nucleus and m_p is the mass of the proton. The $Li^7(p, n)Be^7$ reaction was only used at the reaction threshold to obtain 30-kev neutrons. The $H^3(p, n)He^3$ reaction was used to obtain neutrons ranging in energy from the reaction threshold, about 60 kev, to 1000 kev. The maximum neutron energy for the $H^3(p, n)He^3$ reaction, for which two neutron groups are present at 0°, is 285 kev. Below this energy the pulsed beam prevents interference from the slow neutron group because of its considerably longer flight time. The low average neutron flux, together with high peak flux, results in a low background in the scintillator. An incidental advantage of the pulsed proton beam is the long life of the 0.2-mil aluminum window of the tritium target, or a long life for the lithium target.

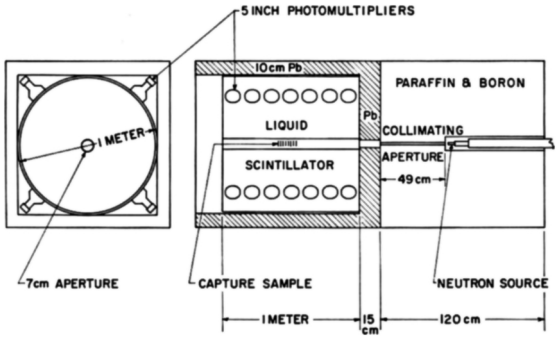

FIG. 1. End view and cross section of the scintillator, neutron source, and shielding. A collimated and pulsed beam of neutrons is passed through the target at the center of the scintillator.

Figure 1 shows the arrangement of neutron source, collimator, scintillator, and shielding. This apparatus has been used, at this laboratory, for radiative capture cross section measurements and has been described by Diven *et al.* (*3*). The scintillator tank is a cylinder 1 meter long and 1 meter in diameter. It is filled with a mixture of toluene, terphenyl, POPOP (wavelength shifter), and cadmium propionate. The scintillating solution is viewed by twenty-eight 5-in. DuMont 6364 photomultiplier tubes connected in parallel.

A target of the isotope whose α is to be measured is placed in the center of the scintillator. Through this target is passed the pulsed beam of fast neutrons collimated so as not to enter the scintillating volume. The U^{235} target is composed of 40 discs of 93% U^{235}, each 0.75 in. in diameter, 0.005 in. thick (9.5 gm/cm^2 total), and spaced 0.12 in. apart in a light aluminum frame. Each disc is suspended by two 0.005-in. steel wires and an 0.008-in. steel helical spring. A similar set of 0.010-in. polyethylene discs, used to produce scattering only, is mounted in the same way.

The U^{233} is in the form of U_3O_8 pellets, packed into aluminum cans. The U^{233} is contaminated with about 1 part in 10^9 of U^{232}. The cans are 0.75 in. in diameter and 0.053 in. in depth. The thickness of the aluminum is 0.002 in. There are seven cans 0.625 in. apart in a sealed stainless steel cylinder. The ends of the stainless steel cylinders, through which the neutron beam passes, are 0.005 in. thick. Thin aluminum flanges on the cans center the sample pellets on the axis of the cylinders. The scattering mockup used to simulate the U_3O_8 neutron scattering is in the form of bismuth oxalate pellets packed into aluminum cans. The physical characteristics of the pellets, cans, and stainless steel cylinder of the mockup are identical to those of the U_3O_8 target.

The Pu^{239} target consists of 22 discs of a Pu^{239}-Al alloy (3% Al by weight) each 0.75 in. in diameter, 0.005 in. thick. The discs are supported in a stainless steel container similar to that used for the U^{233} target. The neutron scattering mockup used in conjunction with the Pu^{239} target consists of polyethylene discs, also mounted in a stainless steel container.

A U^{235} fission counter, which may be inserted in

the 2.5-in. diameter central hole of the scintillator in place of the target, has 36 surfaces, each coated with about 1.2 mg/cm^2 of U^{235}. A U^{233} fission counter has 4 surfaces each coated with about 1 mg/cm^2 of U^{233}. A Pu^{239} fission counter has 9 surfaces each coated with about 1 mg/cm^2 of Pu^{239}.

The characteristics of a large liquid scintillator which make this experiment feasible are the high efficiencies for detection of gamma rays and of neutrons. The efficiencies for the detection of capture and fission by the prompt gamma radiation are assumed to be equal and are close to 100%. The efficiency for the detection of gamma radiation is discussed in more detail by Diven *et al.* (*3*). The efficiency for the detection of fission neutrons was found to be about 90%. This efficiency for neutrons results in a measured probability of 5.3% that no neutron pulse will be observed following a U^{235} fission. Analogous probabilities for U^{233} and Pu^{239} are 4.7% and 2.8%, respectively. To correct the data for this effect, measurements are made with a fission counter in place of the capturing sample. The probability that no detectable neutron pulses follow fission is observed under the same conditions as with the capturing sample, except that coincidences between fission-counter pulses and beam pulses are required to open the 32-μsec gate.

ELECTRONICS

Figure 2 shows a block diagram of the electronics equipment used in the measurement of α. The diagram is simplified in that amplifiers, preamplifiers, delay units, some discriminators, and some scalers are not shown.

The time measurements are made by a time-to-pulse-height converter. It measures the time between a beam pulse and scintillator pulse and puts out a pulse with height proportional to the time interval. Figure 3 shows the output of the time-to-pulse-height converter displayed on a 100-channel pulse-height analyzer. The target for the upper distribution is U^{235}. The target for the lower distribution is the polyethylene scattering mockup. These are plots of counting rate vs. time over a 1-μsec interval. In the upper distribution there is a constant background counting rate on which is superimposed a peak due to fission and capture gamma rays. This peak is produced at the time the beam strikes the target. The background may be interpolated under the peak and thus provides a method of determining the fraction of pulses in the peak which are random and not related to prompt events produced in the scintillator by the neutron beam.

The output of the time-to-pulse-height converter is fed to a single-channel pulse-height analyzer (Fig. 2), centered on the prompt interval. Thus, the single-channel pulse-height analyzer selects those scintillator pulses in coincidence with the beam pulse. The pulse from the single-channel analyzer and the prompt pulse from the scintillator are fed to a coincidence circuit. A discriminator between the

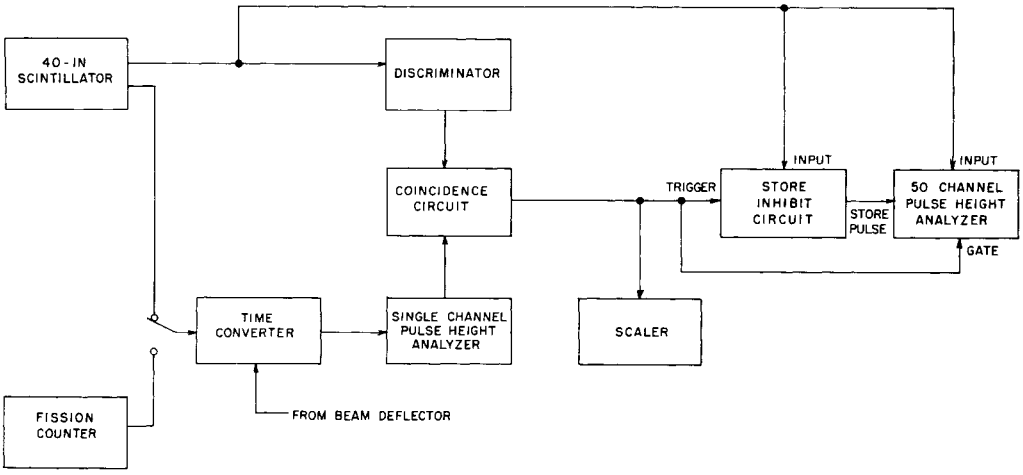

FIG. 2. Block diagram of electronics. The single-channel analyzer following the time converter selects those pulses which occur at "prompt" time (in coincidence with beam pulse). The coincidence circuit selects those prompt pulses of greater than a certain amplitude. These pulses (except for background) are caused by gamma radiation from neutron capture or fission in the target. The trigger pulse is delayed so that the store inhibit circuit is triggered after the prompt pulse. Only those prompt pulses not followed within 32 μsec by other scintillator pulses are stored in the 50-channel analyzer. Fission is nearly always followed by delayed pulses in the scintillator. Therefore, the 50-channel analyzer pulse-height distribution is made up largely of neutron capture events.

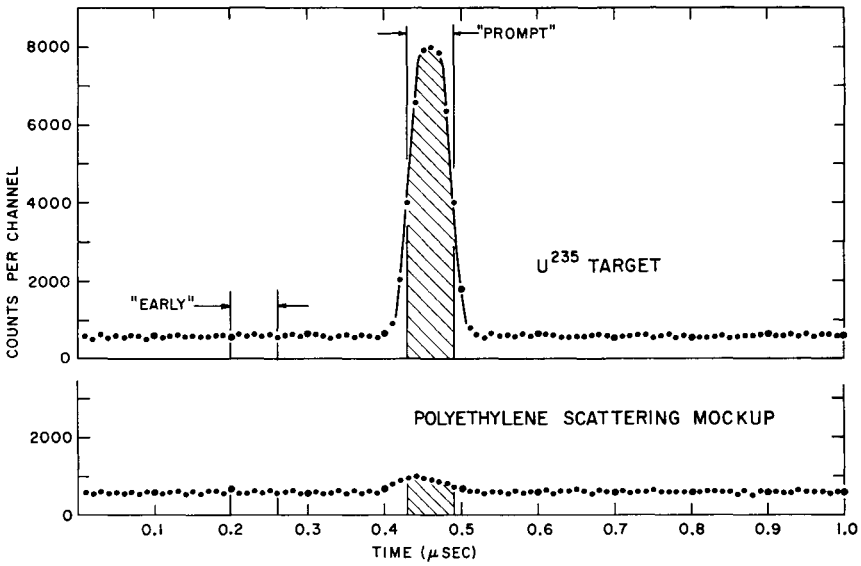

FIG. 3. Time distributions of scintillator pulses with the U^{235} sample and with the polyethylene scattering mockup in the scintillator. For the U^{235} data the prompt channel includes the pulses due to radiative capture and fission. For the polyethylene run the prompt channel includes the pulses due to prompt capture, in the scintillator, of the scattered neutrons. The "early" channels contain background pulses.

scintillator and the coincidence circuit accepts only those scintillator pulses above some fixed level. The coincidence pulse is then used to trigger the store inhibit circuit and to gate on a 50-channel analyzer. Meanwhile the 50-channel pulse-height analyzer has analyzed, but not stored, the prompt pulse from the scintillator. The store inhibit circuit is a logic circuit that makes the decision whether or not to store the analyzed prompt pulse in the 50-channel pulse-height analyzer. A prompt pulse triggers the store inhibit circuit 32-μsec gate. If no scintillator pulses follow the prompt pulse within 32 μsec, the analyzed pulse is stored. However, if any scintillator pulses do follow the prompt pulse within 32 μsec, the analyzed pulse is not stored. Thus the 50-channel pulse-height analyzer displays those pulses occurring at prompt time that are not followed by delayed pulses in the scintillator. These pulses are mostly due to capture events. The trigger pulses, which are counted by a scaler, include all captures and fissions.

Delayed pulses from capture *in the scintillating solution* of fission neutrons, or background radiation, can produce a pulse within 32 μsec after a prompt pulse. A correction was made for the effect of background radiation. Sixty μsec after the end of the 32-μsec gate, another gate is triggered internally. This delayed, or background, gate is also open for 32 μsec. Since the internal triggers are not caused by scintillator pulses, no pulse appears in the 50-channel analyzer associated with the background gates. However, if any scintillator pulses occur during the internally triggered (background) gate, a background scaler (not shown in Fig. 2) is tripped. From the total number of triggers and the number of background triggers followed by scintillator pulses, the fraction of prompt gates containing background radiation pulses from the scintillator is determined. This fraction is denoted by $1 - B_0$.

Background radiation can also produce prompt triggers. A single-channel pulse-height analyzer, not shown in Fig. 2, centered on an interval of the time spectrum just preceding a beam pulse, is used to correct for this effect. The interval selected by the single channel analyzer is called the "early" interval and is shown in Fig. 3.

The fission counter, mentioned earlier, is also shown in Fig. 2. The fraction C_0 of fissions not followed by delayed pulses in the scintillator was measured by inserting the fission counter in the center of the scintillator. During the fission counter runs the fission counter output is connected to the time converter input. The single-channel pulse-height analyzer then selects those fission events in coincidence with a beam pulse. A coincidence between the scintillator and the fission counter is also required. A coincidence between the scintillator, fission counter, and beam pulse establishes the fact that a fission took place and the gate is then opened. For the fission counter runs the 50-channel analyzer displays the scintillator prompt pulse-height distribution of those fissions not followed by delayed pulses in the scintillator.

ANALYSIS

A cycle of measurement at one neutron energy for one isotope consists of identical runs with a fissionable target and with a neutron scattering mockup target. For each of these runs there is the scintillator pulse-height distribution for those pulses occurring at "prompt" time not followed by delayed pulses, and for those pulses occurring at an "early" time not followed by delayed pulses. From the background scaler, mentioned earlier, and the total number of triggers, the fraction of store inhibit gates with one or more background pulses, $1 - B_0$, is determined. From the numbers of prompt trigger pulses and of early trigger pulses the number of triggers at prompt time associated with the beam was determined. For each run the "early" effect was subtracted from the appropriate "prompt" effect.

After subtracting the pulse-height distribution association with the "early" time interval from the pulse-height distribution associated with the "prompt" interval, the resultant distribution was divided by B_0 to correct for background radiation occurring within the 32-μsec gate. The data obtained with the scattering mockup target were then subtracted from the appropriate fissionable sample data.

The counting rates were all low, the capture plus fission being 40 pulses per second. The maximum counting rate for the 50-channel analyzer was 10 pulses per second.

The pulse-height distribution remaining after the background subtractions and corrections for B_0 is ascribed to captures plus C_0 times the total number of fissions. The prompt triggers, with the "early" triggers subtracted, are ascribed to captures plus fissions.

If all of the pulses analyzed by the 50-channel pulse-height analyzer are stored (e.g., if the input to the store inhibit circuit is removed), the pulse-height distribution for captures plus fissions is obtained. Two typical examples for the spectra obtained are shown in Fig. 4 for U^{235} at 400-kev neutron energy. The capture plus C_0X (fissions) curve consists mostly of capture events. The C_0X (capture-plus-fission) curve consists mostly of fission events. Capture gamma rays produce a pulse corresponding to the sum of the energies of the gamma rays, which is equal to the binding energy of a neutron (6.29 Mev in U^{236}), plus the kinetic energy of the incident neutron. For an incident neutron energy of 400 kev, the maximum total energy of the gamma radiation is 6.7 Mev. The mean total energy emitted as gamma radiation by a fissioning U^{236} nucleus is about 7.2 Mev (*4*). The multiplicity of the photons emitted in a radiative capture is different from the multiplicity of the photons emitted in fission. The mean energy of the photons emitted in fission is about 1 Mev, whereas the mean energy of the photons emitted in slow neutron capture is about 2 Mev (*5*). The different multiplicity and average energy for capture and fission events results in a difference in the pulse-height distributions.

The only purpose of the pulse-height distribution

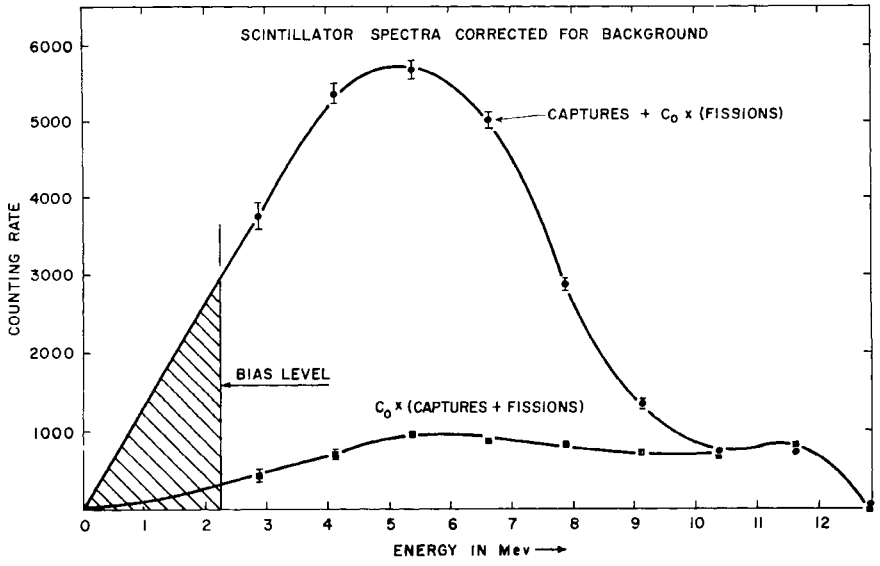

FIG. 4. Pulse-height distributions for capture plus C_0X (fissions) and for C_0X (captures plus fissions). The capture plus fission curve was normalized by multiplying by the C_0 obtained from fission counter data.

is to permit an estimate of the number of pulses below the bias, indicated in Fig. 4. Discriminators on the 50-channel pulse-height analyzer, time converter, store inhibit circuit, and between the scintillator and coincidence circuit were adjusted to eliminate pulses of less than a certain energy. The selection of the bias level was determined by several factors: background counting rate, background spectrum, and incident neutron energy. For an incident neutron energy of 1 Mev, a bias level of greater than 1 Mev was needed to eliminate prompt pulses due to neutron scattering. In all cases the discriminators were set above 1 Mev. Without a proton beam or target in the scintillator, a background counting rate of 1200 counts per second above 2 Mev was present in the scintillator. This was due to radioactivity in the vicinity of the scintillator and to cosmic radiation. A most serious source of background radiation in the case of U^{233} and Pu^{239} targets is the natural activity of the decay products. The U^{233} target was contaminated with about one part in 10^9 of U^{232}. ThC″ in the U^{232} decay chain, with a gamma ray energy of 2.6 Mev, necessitated a high bias. The store inhibit bias remained fixed at 1.6 Mev. The time converter bias was always somewhat lower than the 50-channel analyzer bias. The maximum 50-channel analyzer bias was 4 Mev for U^{233}. Most of the 50-channel pulse-height analyzer data were taken with a 2.25-Mev bias. The highest biases were used at the lowest neutron energies. The useful neutron flux was low at the lowest energies, and the ratio of effect to background was also low. At each energy the biases were lowered until the statistical deviation of the low energy points of the pulse-height distribution, with background subtracted, became comparable to the values of the points.

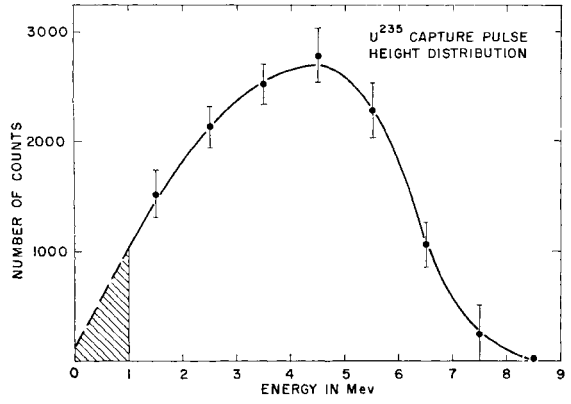

FIG. 5. Capture pulse height distribution for U^{235}, at 400 kev neutron energy corrected for background radiation and for those fissions not followed by delayed pulses in the scintillator. Capture pulse height distributions for U^{233} and Pu^{239} have a similar shape.

TABLE I

EXPERIMENTAL VALUES OF α, THE RATIO OF NEUTRON CAPTURE TO NEUTRON INDUCED FISSION CROSS SECTIONS[a]

E_n(kev)	$\alpha = \sigma_c/\sigma_f$		
	U^{233}	U^{235}	Pu^{239}
30 ± 10	0.109 ± 0.022	0.376 ± 0.036	0.343 ± 0.038
60 ± 15	0.110 ± 0.025	0.327 ± 0.024	0.145 ± 0.017
175 ± 25	0.098 ± 0.020	0.224 ± 0.017	0.142 ± 0.023
250 ± 50	0.091 ± 0.022	0.213 ± 0.016	0.106 ± 0.016
400 ± 90	0.078 ± 0.010	0.152 ± 0.011	0.089 ± 0.009
600 ± 76	0.062 ± 0.009	0.143 ± 0.011	0.065 ± 0.009
750 ± 70	0.047 ± 0.009	0.128 ± 0.010	0.046 ± 0.010
900 ± 63	0.050 ± 0.008	0.101 ± 0.011	0.035 ± 0.012
1000 ± 58	0.030 ± 0.008	0.087 ± 0.008	0.027 ± 0.007

[a] Neutron energies and energy spreads are indicated.

Figure 5 demonstrates how the pulse height distributions were extrapolated to zero energy. Figure 5 shows the capture pulse height distribution for U^{235}, at 400 kev neutron energy, corrected for background radiation and for those fissions not followed by delayed pulses in the scintillator. Similar curves, with poorer statistics and slightly higher discriminator biases, were taken for U^{233} and Pu^{239}. For all three isotopes, however, the distributions when extrapolated to zero energy passed through or near zero counting rate. The actual extrapolations were made from curves similar to that shown in Fig. 4. that were taken for each isotope at every incident neutron energy. Provided that the fraction of pulses below the biases were the same for captures plus C_0X (fissions) as for capture plus fissions, no error would be made by neglecting those pulses below the bias. However, the fractions below the biases differ by a factor of about 1.035. An error of ±0.035 is assigned to this factor. The error was calculated by assuming that the distribution below 1 Mev could either drop to zero immediately or continue at a constant counting rate. Except at very low neutron energies where a high bias was used for U^{233} and Pu^{239}, the error associated with the extrapolation of the pulse-height distribution to zero energy was significant only for U^{235}, where the value of α is the highest. In this case the error due to the extrapolation was less than about 25% of the error due to the statistical uncertainty related to the number of events observed.

From estimates of the number of pulses below the bias, the total number of captures plus C_0X (fissions) and captures plus fissions was determined.

TABLE II

THE RADIATIVE NEUTRON CAPTURE CROSS SECTION σ_c AS A FUNCTION OF INCIDENT NEUTRON ENERGY[a]

E_n (kev)	σ_c (barns)		
	U^{233}	U^{235}	Pu^{239}
30	0.425 ± 0.092	1.031 ± 0.129	0.760 ± 0.104
60	0.331 ± 0.079	0.703 ± 0.076	0.273 ± 0.039
175	0.236 ± 0.051	0.347 ± 0.038	0.241 ± 0.044
250	0.214 ± 0.054	0.301 ± 0.033	0.177 ± 0.030
400	0.176 ± 0.027	0.198 ± 0.021	0.138 ± 0.024
600	0.124 ± 0.020	0.172 ± 0.019	0.108 ± 0.017
750	0.093 ± 0.019	0.150 ± 0.017	0.077 ± 0.018
900	0.097 ± 0.017	0.128 ± 0.017	0.061 ± 0.021
1000	0.058 ± 0.016	0.109 ± 0.011	0.048 ± 0.013

[a] The capture cross section was calculated from the experimental values of the fission cross section and α. The uncertainties are due to the standard deviations in α and the fission cross sections.

The fission counter data provided values of C_0 at one energy. From the average number of neutrons emitted per fission, $\bar{\nu}$, distribution in number (*6*, *7*), and the change in $\bar{\nu}$ with energy, C_0 was calculated for all energies. C_0 is a slowly varying quantity. It changes by only 10% from 30 kev to 1 Mev for U^{235}. These data provided values of α, the ratio of the number of capture events to the number of fission events for each isotope and incident neutron energy.

The U^{235} data was corrected for the 7% U^{238} contamination in the sample. The actual value of this correction depends upon the incident neutron energy. Roughly, however, it is about 7% of α.

RESULTS

The experimental values of α are shown in Table I. From the experimental values of α and of the fission cross section (*8*), the capture cross section, σ_c, was calculated for each incident neutron energy and isotope. The values of σ_c are given in Table II. The standard deviations for α are a combination of statistical uncertainties related to the number of events observed and estimates of the uncertainties in the extrapolation of the spectra to zero energy. The neutron energy spread is due to the tritium target thickness and the time resolution of the timing circuits. All data except those at 30 kev were taken with the T(p, n)He^3 reaction. The three values at 30 kev were taken with the Li^7(p, n)Be^7 reaction. The uncertainties assigned to the capture cross section values are due to the standard deviations assigned to α and the fission cross sections.

DISCUSSION

Figure 5 shows the results of the present experiments for U^{233}. Almost no data are available for comparison. Spivak *et al.*, as quoted in ANL-5800 (*9*), obtained values of η at 30 kev, 140 kev, 250 kev, and 900 kev using photoneutron sources (Sb + Be, Ca + D_2O, and Na + Be, respectively). The precision of these measurements, however, is insufficient for a determination of α. Yiftah, *et al.* (*10*) mention an estimate based on meager resonance level data that the U^{233} capture cross section is about two-thirds the U^{235} capture cross section. This appears to be a reasonably good assumption.

Multiplying the α for U^{235}, shown in Fig. 6, by the fission cross section quoted by Hughes and Schwartz (*8*), the radiative capture cross sections are obtained. These are shown, with previously obtained capture cross sections, in Fig. 7. Not shown in this figure are EBR-1 data of Kafalas *et al.* (*11*). Yiftah *et al.* (*10*) summarize the EBR-1 data in conjunction with other U^{235} neutron capture data. Spivak *et al.* (*9*) measured η using photoneutron sources and computed α and σ_c. The ORNL data (*10*, *12*) are from a comparison of the total absorption cross section of U^{235} to the capture cross section of indium. The absorption cross section, σ_a, of U^{235} was then normalized to $\sigma_a = \sigma_f(1 + \alpha) = 1.77$ barns at 175 kev. The data from the present experiment yields $\sigma_a = 1.92 \pm 0.03$ at 175 kev. If the ORNL data were normalized to this higher value, they would be compatible with the present data. The KAPL data

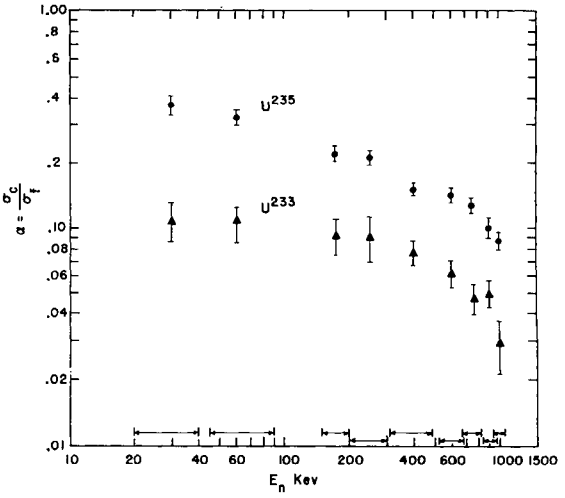

FIG. 6. The ratio of neutron capture to fission cross sections, α, is plotted as a function of incident neutron energy from 30 to 1000 kev for U^{233} and U^{235}. The horizontal arrows indicate the incident neutron energy spread.

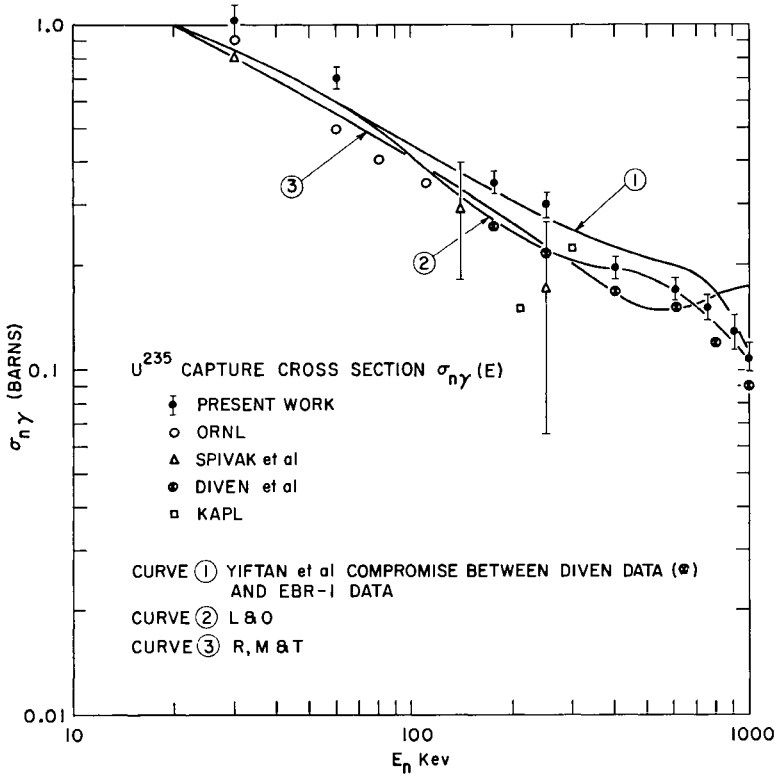

FIG. 7. The experimental values for the radiative capture cross section from U^{235} are plotted as a function of the incident neutron energy from 10 to 1000 kev.

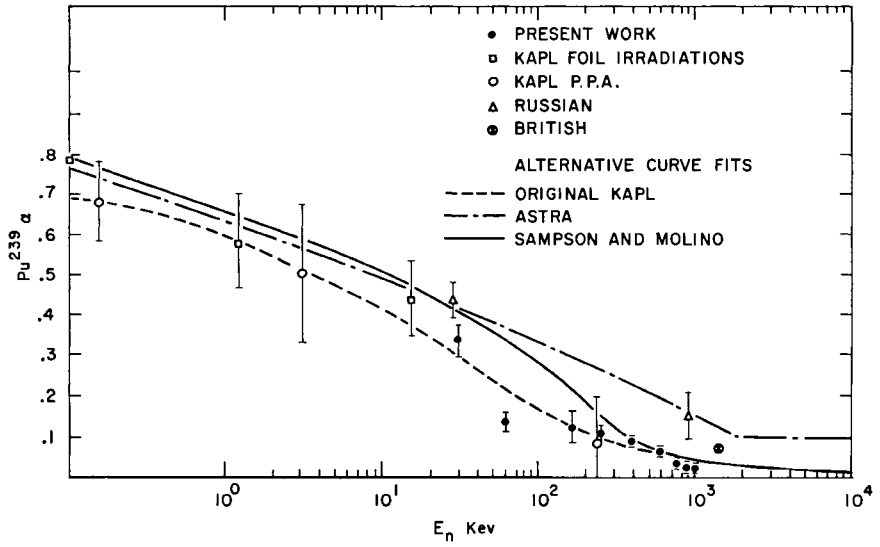

FIG. 8. The experimental values for α, the ratio of neutron capture to fission cross sections, for Pu^{239} are plotted as a function of the incident neutron energy. The various curves are from an analysis of the previous data by Sampson and Molino.

(*9*) were obtained with appropriately shielded foils and mass spectrometer analysis.

The most accurate earlier measurement of the capture cross section for U^{235} was that of Diven *et al.* (*2*) using the same techniques as used here. The present experiment is more accurate, however, because the scintillator used has 8 times the volume of the previous one. With the larger scintillator the efficiency for the detection of both gamma rays and neutrons is much higher. Because of the high neutron

efficiency, C_0 and the error in C_0 are much smaller than those previously obtained. Because of the higher efficiency for gamma-ray detection, the extrapolation of the pulse-height distribution to zero energy is more exact.

The most important of these effects is the latter. In the earlier experiment which was performed in 1956 the electronics equipment was less sophisticated than it is now. It was not possible previously to obtain a pulse height spectrum from capture events. Instead, the ratio of the number of detected capture events to the number of detected fission events was taken for three widely spaced biases and from these ratios, an extrapolation to zero bias was made. It was realized that this was a risky procedure and, as discussed in ref. *2*, the uncertainty in this extrapolation contributed the major portion of the quoted error. Since 1956 much experience has been obtained in observation of pulse height spectra from capture events in the 19 in. scintillator used in the 1956 measurements as well as in the (40 in.) scintillator used in the present experiments. From the pulse height spectra published in ref. *3*, it is clear that the extrapolation to zero pulse height made in ref. *2* was not valid since the detailed shape of the pulse height spectra of capture and fission pulses are different from those assumed in ref. *2*. Furthermore sufficient data are available from the experimental work of ref. *3* to renormalize the old values of α. We find that the multiplicative factor necessary to correct for the pulse height distribution below the 1.25 Mev bias for the 19 in. scintillator is $1.20^{+.08}_{-.04}$ as compared to the previously assumed 1.08 ± 0.08. The old values should therefore be raised by about 11% which brings them into agreement with the present measurement. The accuracy of these corrected results is not great, however, because of the magnitude of the correction. Corresponding to the 20% correction in the extrapolation from 1.25 Mev to zero bias with the 19 in. scintillator is a 3.5% correction with the 40 in. scintillator.

Three curves are shown in Fig. 7. Curve 1 is that adopted by Yiftah *et al.* (*10*) as a compromise between the earlier Diven data and the EBR-1 data. Curve 2 is that of Loewenstein and Okrent as quoted by Yiftah *et al.* (*10*). Curve 3 is that calculated by Rae *et al.* (*13*). Curve 3 rises between 400 kev and 1000 kev and then decreases again. Rae *et al.* have pointed out that by assuming energy level bands above 500 kev in addition to the experimentally observed ones, the curve could be brought down to follow the data.

An analysis of the previous data on α for Pu^{239} was made by Sampson and Molino (*14*). Figure 8 shows the results of this analysis with the data from the present experiment. Sampson and Molino conclude that α undergoes a sharp decrease with energy near 100 kev. The results of the present experiment indicate a sharp decrease in α near 60-kev neutron energy. With the exception of the 60-kev datum, the present results are consistent with the original KAPL curve quoted by Sampson and Molino.

ACKNOWLEDGMENTS

We would like to acknowledge the many helpful discussions with Dr. James Terrell. Mr. David Garelick, a summer student from MIT, aided greatly in the initial phases of the research. Mr. Alfred Koelle is responsible for the excellent electronic components peculiar to this experiment. Mr. John W. Jordan and the P-3 staff designed and built much of the experimental equipment.

REFERENCES

1. H. A. BETHE, *Proc. Intern. Conf. Peaceful Uses Atomic Energy, Geneva, 1955*, **4**, 321 (1956). United Nations, New York.
2. B. C. DIVEN, J. TERRELL AND A. HEMMENDINGER, *Phys. Rev.* **109**, 144–150 (1958).
3. B. C. DIVEN, J. TERRELL AND A. HEMMENDINGER, *Phys. Rev.* **120**, 556–569 (1960).
4. F. C. MAIENSCHEIN, R. W. PEELLE, W. ZOBEL, AND T. A. LOVE, *Proc. Second Intern. Conf. Peaceful Uses Atomic Energy, Geneva, 1958*, **15**, 366 (1958). United Nations, New York.
5. L. V. GROSHEV, A. M. DEMIDOV, V. N. LUTSENKO, AND V. I. PELEKHOV, *Proc. Second Intern. Conf. Peaceful Uses Atomic Energy, Geneva, 1958*, **15**, 138 (1958). United Nations, New York.
6. B. C. DIVEN, H. C. MARTIN, R. F. TASCHEK, AND J. TERRELL, *Phys. Rev.* **101**, 1012–1015 (1956).
7. JAMES TERRELL, *Phys. Rev.* **108**, 783–789 (1957).
8. D. J. HUGHES AND R. B. SCHWARTZ, Neutron cross sections, Brookhaven National Laboratory Report BNL-325, Suppl. 1, Superintendent of Documents, U. S. Government Printing Office, Washington, D. C. (1957).
9. Reactor physics constants. Argonne National Laboratory Report ANL-5800 (1958).
10. S. YIFTAH, D. OKRENT, AND P. A. MOLDAUER, "Fast Reactor Cross-Sections," pp. 80–88. Pergamon Press, New York, 1960.
11. P. KAFALAS, M. LEVENSON, AND C. M. STEVENS, *Nuclear Sci. and Eng.* **2**, 657–663 (1957).
12. R. L. MECKLIN, P. D. MILLER, J. H. NEILER, AND J. H. GIBBONS, *Bull. Am. Phys. Soc.* **Ser. II, 4**, 385, (1959); J. A. HARVEY, Reports to the AEC Nuclear Cross Sections Advisory Group, October 28-29, 1959, WASH-1026 (October, 1959).
13. E. R. RAE, B. MARGOLIS, AND E. S. TROUBETZKOY, *Phys. Rev.* **112**, 492–497 (1958).
14. J. B. SAMPSON AND D. F. MOLINO, An α_{49} (E) curve consistent with EBR-1 measurements and also with most former measurements. Knolls Atomic Power Laboratory Report KAPL-1793 (May, 1957).

NUCLEAR SCIENCE AND ENGINEERING: **12**, 178–184 (1962)

Backscattering of Gamma Rays

TOMONORI HYODO

Department of Nuclear Engineering, Kyoto University, Kyoto, Japan

Received April 18, 1961

Spectra of backscattered radiation from semi-infinite slabs of paraffin, aluminum, iron, tin, and lead were measured by means of a scintillation spectrometer, as a function of the measuring angle θ, which is the angle between the normal to the plane face of the slabs and the detector axis. The point gamma sources of Co^{60} and Cs^{137} were placed in close contact with the scattering slabs. By using this geometry the measurement was performed without perturbing effects produced by detector or source collimating shields. The energy and number albedos, the angular distributions of scattered energy and number of photons, and the energy distributions are given for each combination of gamma source and scatterer.

INTRODUCTION

The spectral distribution of gamma rays from a point source is modified when the source is placed on a semi-infinite, homogeneous medium. This phenomenon is caused by the backscattering of gamma rays. Rather little is known experimentally about the angular and energy distribution of scattered gamma rays and the albedo. With the recent development of the scintillation spectrometer, particularly the multichannel pulse-height analyzer, and improved methods for handling the data, it seems that more precise measurement might be possible. The only geometrical condition under which the albedo against a semi-infinite medium can be completely measured, without perturbing effects produced by detector or source collimating shields, is the arrangement in which an isotropic source is placed on the scatterer. We have studied backscattering phenomena with this arrangement.

Hayward and Hubbel (*1*) investigated the radiation backscattered by semi-infinite slabs of wood and steel wool when irradiated by collimated Co^{60} gamma rays, by means of a scintillation spectrometer. Heine and McCall (*2*) measured scattered gamma rays as a function of the energy of the primary gamma radiation and geometry by means of a scintillation spectrometer. These were very excellent pioneer investigations at a time when only a small number of theoretical calculations had been carried out and measuring instruments were under development. Absolute values of the energy albedo of various materials for collimated gamma rays from Co^{60} and Au^{198} have been determined experimentally by Bulatov and Garusov (*3*). They measured scattered gamma rays with a specially constructed G-M counter, and the photon energy was measured by means of the absorption method.

The present investigation is concerned with spectral modification of the 0.662-Mev gamma rays of Cs^{137} and the 1.173- and 1.332-Mev gamma rays of Co^{60} caused by backscattering from semi-infinite media of paraffin, aluminum, iron, tin, and lead. The point source was placed in very close contact with the scatterer. A series of pulse-height distributions using a geometry designed to show up any variation in the photon energy distribution as a function of angle θ have been measured by means of a scintillation spectrometer. The response-corrected spectra have been obtained with the help of the response function matrix (*4–6*).

The number albedos, the energy albedos, and the angular and energy distributions of scattered photons are given in this paper for each combination of gamma source and scatterer.

EXPERIMENTAL ARRANGEMENT AND PROCEDURE

The gamma sources of Co^{60} and Cs^{137} were prepared by evaporation of drops of solution of high specific activity on very thin mica plates, approximately 10 mg/cm^2, and covered with cellophane tape. These mica plates were supported by steel wires. The in-

tensities of the sources of Co^{60} and Cs^{137} were approximately 13 and 20 μC respectively.

The scatterers used in this experiment were paraffin, aluminum, iron, tin, and lead. Prior to the systematic research on the backscattering of gamma rays, it was necessary to clarify from what region the scattered gamma rays emerged, since there were no data available concerning the size of scatterer considered as semi-infinite. A preliminary experiment was carried out (7), and the size of the scatterer was determined as shown in Table I. The outline of this experiment is described in the Appendix.

Figure 1 shows the measuring geometry used in this investigation. The scintillation head with lead shield was placed on a stand which could be rotated at a fixed radius. The detector axis of the spectrometer was set at given value of θ, the angle between the normal to the face plane of the scatterer and the detector axis, with the aid of an index plate. Data were obtained for each scatterer at 10° intervals of the angle θ, from 0° to 90°. The maximum possible error in a specified value of θ was less than 0.2 deg.

The source was placed at the center of the goniometer and on the scintillator axis. The distance between the source and the front face of the scintillator was 40 cm. The scatterer was placed in very close contact with the source.

TABLE I

SCATTERERS

Scatterer	Necessary size		Scatterer in use	
	Thickness (cm)	Diameter (cm)	Thickness (cm)	Diameter or latera (cm)
Paraffin[a]	16	40	40	50 × 50
Aluminum	7	30	12	50 × 45
Iron	3	25	5.0	40 × 40
Tin	3	20	3.0	20ϕ
Lead	1.6	10	3.0	20ϕ

[a] The density is 0.919 gm/cm³; the fractions of the elements are 14.85% for hydrogen and 85.44% for oxygen.

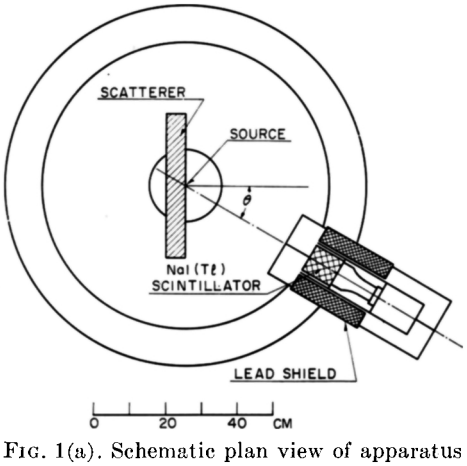

FIG. 1(a). Schematic plan view of apparatus

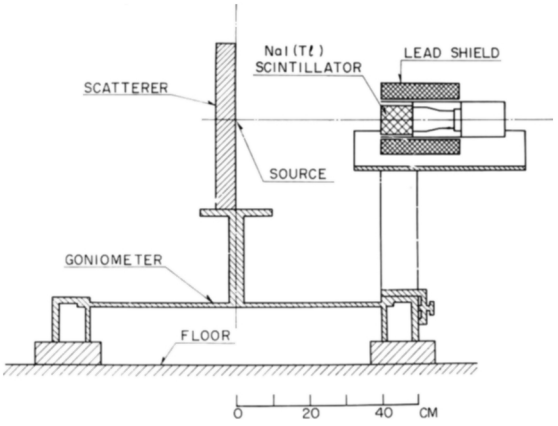

FIG. 1(b). Schematic elevation view of apparatus

To carry out the determination of the geometrical efficiency of the detector assembly, a point source of Cs^{137} was moved in the plane at a distance of 40 cm from the scintillator face. The results of the experiment showed that the detection efficiency of the detector assembly with the source placed at a point on the front face of the scattering slab 10 cm away from the scintillator axis is nearly the same as its value when the source is placed at the intersection of the scintillator axis and the front face of the scattering slab.

The scintillation head consists of a 3-in. diameter by 3-in. long NaI(Tl) scintillator together with a photomultiplier tube type 6363 and a cathode follower mounted in a single unit. The high voltage power supply is regulated by a parallel circuit consisting of 85A2's connected with a type 6146 vacuum tube. The output pulses of the scintillation head are amplified by an Argonne type A-61 amplifier and fed to a core memory type, 400 channel, pulse-height analyzer.

The location of the photopeak and the base line have been tested for each measurement, and the stability of this device against drift in channel width and base line has proved to be very good.

The resolution and linearity of the instrument was excellent. The pulse-height distribution produced by the Cs^{137} source used in this investigation was compared with that obtained using a source having only one tenth as great an intensity, and there was no difference between the two results.

Since the "Live Time" meter of the spectrometer is controlled by a 100 kc/s crystal oscillator, the time measurement in this experiment was very accurate.

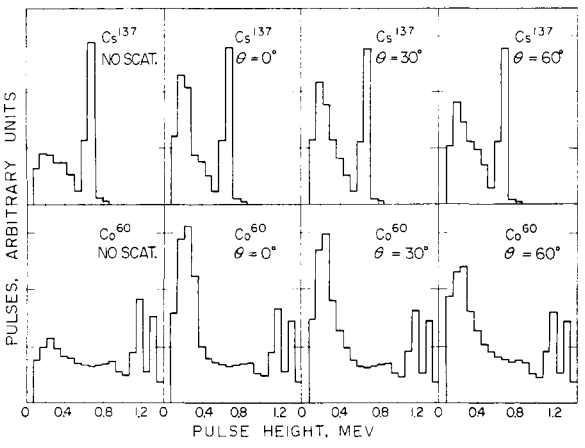

FIG. 2. Examples of the observed pulse height distributions of gamma rays incident on the scintillator. The scatterer was iron. The data labeled "NO SCAT." were obtained without the scatterer.

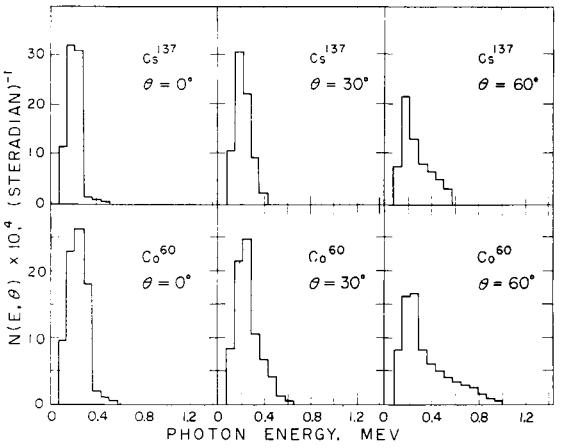

FIG. 3. The energy-angle distribution $F(E, \theta)$ for the iron scatterer. The values are number of photons in the energy interval of width 72 kev.

In a series of separate experiments (*6*), the response of a NaI(Tl) scintillator, 3-in. diam and 3-in. long, to collimated, axially incident gamma rays had been studied and expressed as a 20 by 20 matrix for the energy 0 to 1.440 Mev. The matrix was inverted on an automatic computer for ease of application to spectra. For the purpose of correction of a measured pulse-height distribution by the inverted matrix M_{ij}^{-1}, the pulse-height distribution must be divided into 72-kev intervals, as in the case of the pulse-height interval of the response function matrix, and this is designated as P_j. The response corrected spectrum N_i is obtained from the product of P_j and M_{ij}^{-1} as

$$N_i = \sum_{j=1}^{N} P_j M_{ij}^{-1} \tag{1}$$

The application of this matrix will be discussed in the following sections.

DATA AND RESULTS

Figure 2 shows, in histogram form, examples of the observed pulse-height distribution of the gamma rays incident on the detector from the source directly, together with the scattered radiation from the scatterer. The data labeled "NO SCAT." were obtained without the scatterer. The spectrum was obtained by subtraction of the response-corrected spectrum without scatterer from that with scatterer, and the following corrections had to be made:

A correction was made for the absorption of gamma rays by the material at the source end of the scintillator[1] (*8*). A correction also had to be made for the variation of the geometry of this experiment from that used in the measurement of the input data for the response function of the scintillator. The effect of this modification on the spectrum of gamma rays directly incident on the scintillator was corrected automatically as a result of the subtraction of the spectrum without the scatterer from that with the scatterer. For the scattered radiation, the correction was made for the variation of efficiency with the change of the source position. Since the variation of the pulse-height distribution in the two geometries might be trivial for the low energy gamma rays, the correction was not made in this region.

The spectra of a number of photons in each 72-kev interval were normalized for unit solid angle and for one primary photon incident to the scatterer; thus the energy-angle distribution of scattered gamma rays $N(E, \theta)$ was obtained. Several examples of $N(E, \theta)$ for the iron scatterer are shown in Fig. 3.

The angular distribution of scattered photons, $A(\theta)$, the angular distribution of reflected energy, $A_E(\theta)$, the energy spectrum, $A(E)$, the albedo, A, and the energy albedo, A_E, were calculated using the following formulas:

$$A(\theta) = \sum_{i=1}^{20} N(E_i, \theta) \tag{2}$$

$$A_E(\theta) = \sum_{i=1}^{20} \frac{E_i}{E_0} N(E_i, \theta) \tag{3}$$

$$\begin{aligned} A(E) = {} & N(E, \theta_0) \int_0^{\Delta\theta/2} 2\pi \sin\theta \, d\theta \\ & + \sum_{k=1}^{8} N(E, \theta_k) \int_{k\Delta\theta-(\Delta\theta/2)}^{k\Delta\theta+(\Delta\theta/2)} 2\pi \sin\theta \, d\theta \\ & + N(E, \theta_9) \int_{9\Delta\theta-(\Delta\theta/2)}^{9\Delta\theta} 2\pi \sin\theta \, d\theta \end{aligned} \tag{4}$$

[1] Private communication from The Harshaw Chemical Company.

$$A = \sum_{i=1}^{20} A(E_i) \tag{5}$$

$$A_E = \sum_{i=1}^{20} \frac{E_i}{E_0} A(E_i) \tag{6}$$

where E_i is the center of the energy interval and θ_k is the angle of measurement

$$E_i = [36 + 72\ (i - 1)]\ \text{kev}$$

$$\theta_k = (10\ k)^\circ \text{ and } 4\ \theta = 10^\circ$$

Tables II through V contain the values obtained in this experiment of $A(\theta)$, $A_E(\theta)$, $A(E)$, A, and A_E, respectively, for the different sources and scatterers.

TABLE II

THE ANGULAR DISTRIBUTION OF SCATTERED PHOTONS[a]

$A(\theta) \times 10^3$ (sterad)$^{-1}$

Source	Scatterer	θ									
		0°	10°	20°	30°	40°	50°	60°	70°	80°	90°
Co^{60}	Paraffin	63	63	63	64	65	68	70	73	72	77
	Aluminum	92	92	92	91	91	89	88	79	57	39
	Iron	77	75	76	74	74	71	73	62	46	13
	Tin	38	38	39	39	40	39	42	39	28	20
	Lead	15	18	21	20	20	28	20	24	25	−3
Cs^{137}	Paraffin	89	88	88	88	89	90	92	91	86	86
	Aluminum	116	115	116	113	111	108	104	90	60	36
	Iron	84	83	83	81	81	77	73	66	42	16
	Tin	37	37	37	37	39	38	38	35	30	8
	Lead	14	14	15	15	15	16	17	15	8	−1

[a] These figures were not corrected for the room scattered gammas and the small angle scattered radiation.

TABLE III

THE ANGULAR DISTRIBUTION OF SCATTERED ENERGY[a]

$A_E(\theta) \times 10^3$ (sterad)$^{-1}$

Source	Scatterer	θ									
		0°	10°	20°	30°	40°	50°	60°	70°	80°	90°
Co^{60}	Paraffin	10	10	10	11	12	14	15	18	22	24
	Aluminum	16	16	16	17	18	19	22	23	20	14
	Iron	14	14	15	15	16	17	20	21	18	5
	Tin	9	9	9	10	11	11	15	16	13	10
	Lead	4	4	5	6	6	10	8	10	12	−1
Cs^{137}	Paraffin	25	24	24	25	26	28	31	34	36	36
	Aluminum	32	32	33	33	34	35	37	35	26	17
	Iron	25	25	26	26	27	28	29	30	21	7
	Tin	13	13	13	14	15	17	18	18	18	5
	Lead	5	5	6	6	6	8	9	8	5	1

[a] These figures were not corrected for the room scattered gammas and the small angle scattered radiation.

TABLE IV

THE ENERGY SPECTRA OF SCATTERED GAMMA RAYS[a]

$A(E) \times 10^3$ (Mev-sterad)

Source	Medium energy of interval (kev)	Scatterer				
		Paraffin	Aluminum	Iron	Tin	Lead
Co^{60}	36					
	108	232	221	83	17	16
	180	184	223	189	48	20
	252	213	231	210	112	37
	324	94	115	101	80	42
	396	60	71	64	52	32
	468	44	54	49	44	28
	540	32	41	41	22	28
	612	27	32	27	22	18
	684	20	23	22	21	17
	756	18	21	19	18	13
	824	11	18	17	16	13
	900	11	13	11	14	8
	972	11	12	11	11	10
	1044	7	8	9	8	4
Cs^{137}	36					
	108	361	340	116	21	17
	180	355	374	303	90	16
	252	231	244	209	115	43
	324	107	116	103	77	34
	396	75	80	72	57	30
	468	50	62	39	41	21
	540	40	43	37	33	18
	612	19	10	20	13	2

[a] These figures were not corrected for the room scattered gammas and the small angle scattered radiation.

ESTIMATE OF ERRORS

The standard deviation of the values of pulse-height distribution in each interval P_j is less than 0.1 %, and that of each element of the inverse matrix of the response function might be 1 %. Those errors propagate in the response corrected spectra so that the standard deviation of their values may be nearly 3 %.

The small angle Compton scattered gamma rays could not be distinguished from gamma rays directly incident on the detector. The rough estimation of these scattered gamma rays was made with the help of the results of Monte Carlo calculations performed by Berger and Raso (*9*). No Monte Carlo values for the incident gamma-ray energies of 0.662, 1.172, and 1.333 Mev were given in their paper, so the values for 0.5 and 1.0 Mev were used. In the case of the iron scatterer, for example, to the data of the number and energy albedo 0.4×10^{-2} and 0.2×10^{-2} had to be added for Cs^{137} and 2.2×10^{-2} and 1.6×10^{-2} for Co^{60} respectively. Corrections of

TABLE V

THE NUMBER ALBEDO A AND THE ENERGY ALBEDO A_E

Scatterer	Number albedo		Energy albedo	
	Cs^{137}	Co^{60}	Cs^{137}	Co^{60}
Paraffin	0.57 ± 0.02	0.46 ± 0.02	0.19 ± 0.01	0.112 ± 0.005
Aluminum	0.59 ± 0.02	0.52 ± 0.02	0.20 ± 0.01	0.136 ± 0.005
Iron	0.42 ± 0.02	0.42 ± 0.02	0.16 ± 0.01	0.120 ± 0.005
Tin	0.22 ± 0.02	0.25 ± 0.02	0.10 ± 0.01	0.088 ± 0.005
Lead	0.09 ± 0.02	0.17 ± 0.02	0.04 ± 0.01	0.059 ± 0.005

approximately the same magnitude must be made for the other scatterers.

There were scattered gammas incident on the detector from all parts of the room, specially from the goniometer. These may be called "room scattered gammas" for the sake of distinguishing them from the gammas scattered from the sample. The room scattered gammas might decrease when the scatterer is placed in contact with the source because of the absorption of primary gamma rays. Overcorrection might be made in this case in the process of subtraction of the spectra without the scatterer from that with scatterer.

The estimation of the room scattered gammas was not easy. The only method of estimation was to compare the energy-angle distribution obtained by experiment with those of Monte Carlo values having sufficient histories. We could not obtain these Monte Carlo values, so a rough estimation was made in the case of Cs^{137} with the aid of the Monte Carlo values of the angular distributions of scattered photons and energy, for the incident energy of 0.5-Mev, obtained by Berger and Raso (*9*). The contributions of the room scattering calculated for lead and tin scatterers were approximately 0.025 and 0.01, respectively, in absolute value. For the other scatterers, experimental values were larger than Monte Carlo values, but correction for the overcorrection of the room scattered gammas might be made for these scatterers. In this paper an absolute value of 0.01 was added to the experimental values of number albedo for all scatterers and sources as the room scattering correction. Their contribution to the energy albedos is considered to be small because of their low energy.

Bremsstrahlung caused by the beta rays from Co^{60} and Cs^{137} was negligible for the scattered gamma rays.

COMPARISON WITH OTHER EXPERIMENTS AND WITH MONTE CARLO VALUES

The geometry of the experiment performed by Bulatov and Garusov (*3*) is different from that of this experiment. Accordingly, their results can not be compared with those of this author.

TABLE VI

MONTE CARLO VALUES OF THE NUMBER AND ENERGY ALBEDO (*9*)

Scatterer	Number albedo				Energy albedo			
	0.5 Mev	Cs^{137}[a]	1.0 Mev	Co^{60}[a]	0.5 Mev	Cs^{137}[a]	1.0 Mev	Co^{6}[a]
Water	0.517	0.50	0.474	0.457	0.192	0.17	0.126	0.106
Concrete	0.447	0.43	0.413	0.383	0.188	0.155	0.120	0.097
Iron	0.305	0.32	0.305	0.30	0.149	0.13	0.105	0.091
Tin	0.149	0.16	0.176	0.17	0.082	0.085	0.075	0.070
Lead	0.053	0.07	0.094	0.10	0.032	0.038	0.045	0.045

[a] These figures are the interpolated values of albedo obtained by Berger and Raso (*9*) which were kindly forwarded by Dr. Eric T. Clarke to the author as a private communication.

Berger and Raso (*9*) performed Monte Carlo calculations. Comparing our results with their 0.5- and 1.0-Mev values shown in Table VI, the former are somewhat larger than the latter in number albedos, but a good agreement is seen between their values of energy albedos and ours. Both results were obtained by the process of cutting off in the region of low energy photons, and if we take into account the complicated phenomena of the absorption and scattering processes, there are no fundamental discrepancies between the two results.

ACKNOWLEDGMENT

The author would like to express his thanks to Prof. S. Shimizu for discussion and encouragement during the course of the work, to Mr. T. Okumura for preparation of the sources and maintenance of the instruments, and to Miss A. Takada for her assistance in the calculations.

APPENDIX

Prior to the systematic research of backscattering of gamma radiation, it became necessary to clarify the matter of what region of the scatterer in contact with a point gamma source was effective for this phenomenon. Few data have been obtained concern-

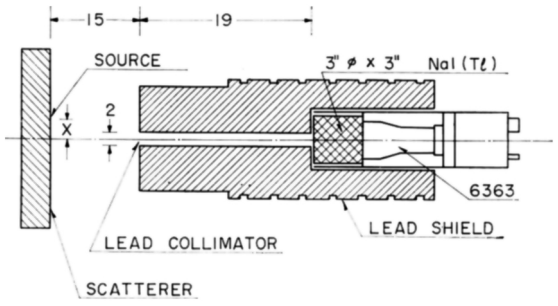

FIG. 4. Experimental arrangement of the preliminary experiment.

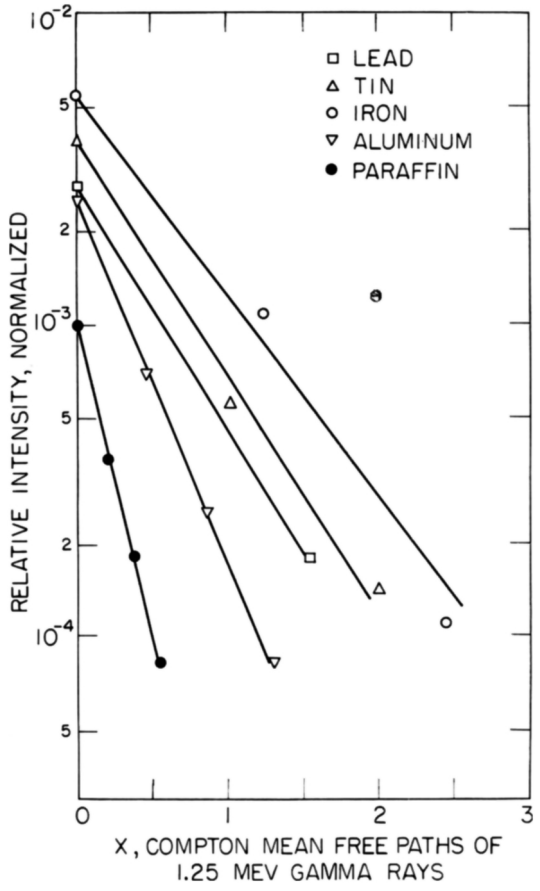

FIG. 5. Integrated intensity of backscattered radiation as a function of the source position, x. A Co^{60} gamma ray source is shifted laterally from the center line of the detector. The integrated intensity of the backscattered radiation, shown by in ordinates, is expressed in units of the ratio of the integrated intensity of the scattered radiation incident on the scintillator to that of directly incident gamma rays from a source at $x = 0$ cm and without any backscatterer.

ing this problem, and so the author determined the necessary size of the scatterer from this experiment. Although the process of measurement and correction of data is described in more detail in the reference cited (7), it is described briefly here.

For the purpose of surveying the intensity of backscattered radiation from the part of the scatterer, the scattered radiation emerging perpendicularly from the surface was measured. The experimental arrangement of gamma ray source, scatterer, and scintillation detector is shown in Fig. 4. A lead collimator which has a cylindrical aperture, 2 cm diam by 29 cm long, was placed in front of the detector assembly described in the preceding sections. The scatterer was placed 15 cm away from the collimator face. The axis of the collimator was perpendicular to the surface of the scatterer. The pulse-height analyzer and associated circuits were identical with that described in the previous sections.

In the first part of the experiment, point sources of Co^{60} and Cs^{137} were displaced along the surface

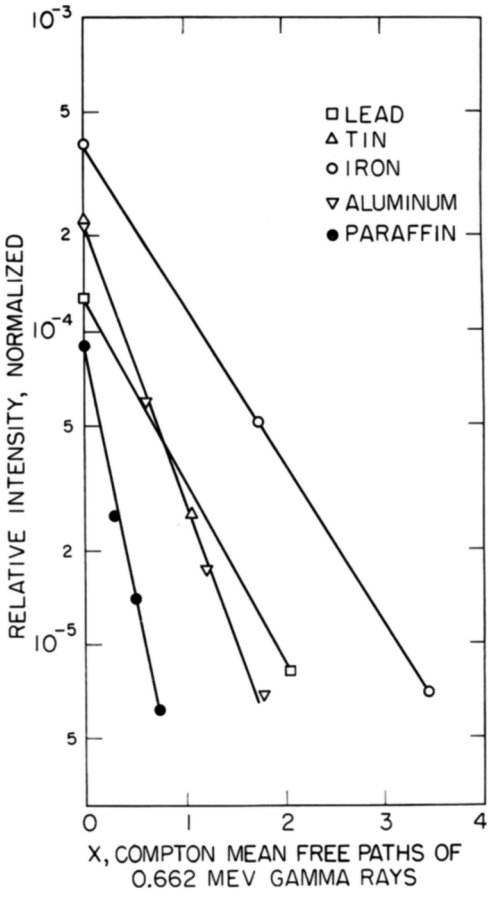

FIG. 6. Integrated intensity of backscattered radiation as a function of the source position, x. A Cs^{137} gamma ray source is shifted laterally from the center line of the detector. The integrated intensity of the backscattered radiation, shown by the ordinates, is expressed in units of the ratio of the integrated intensity of the scattered radiation incident on the scintillator to that of the directly incident gamma rays from a source at $x = 0$ cm and without any backscatterer.

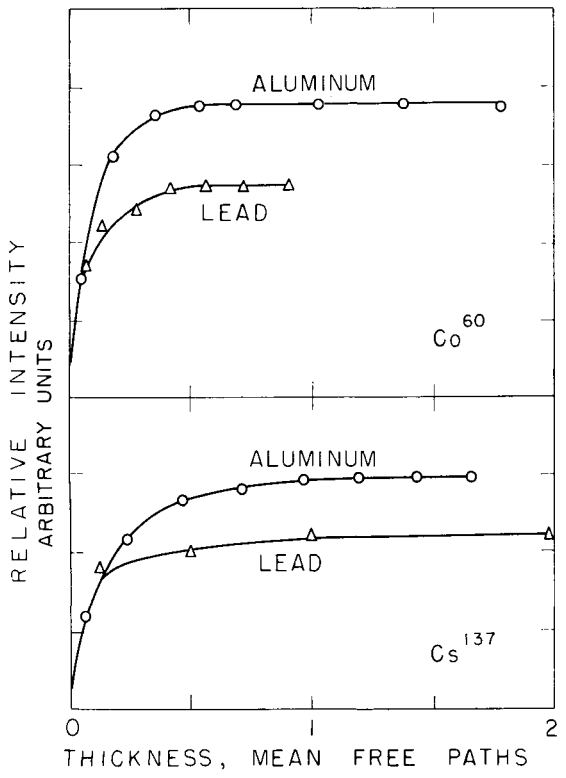

FIG. 7. Measured intensity of backscattered radiation of Co^{60} and Cs^{137} gamma rays incident on the detector as a function of scatterer thickness. The source position is $x = 0$ cm.

plane of the scatterer. Data were obtained for each scatterer and for each 3-cm displacement x of the source from the detector axis up to 15 cm. The background due to the directly incident gamma rays from the source was of course subtracted in each measurement. Furthermore, the contribution of the scattered radiation from the wall of the collimator and the obliquely incident radiation which might penetrate the lead of the collimator and the detector shield to the spectrum had to be eliminated. In order to eliminate these effects, a lead plug was used, which could be inserted exactly into a collimator canal. By observing the difference of the pulse-height distributions with and without this plug, we could subtract the contribution of such undesirable radiation from the observed pulse-height distributions.

It is interesting to note that under the present experimental arrangement the integrated intensity of backscattered radiation incident on the scintillator decreases as x increases, approximately according to a simple empirical formula, $I(x) = I(0)e^{-ax}$. Variation of the value of the constant a with the scattered material is least when the Compton mean free path is taken as the unit of x. Results obtained are given in Figs. 5 and 6. The integrated intensity of the backscattered radiation, shown in the ordinates of the figures, is expressed in units of the ratio of the integrated intensity of scattered radiation incident on the detector to that of directly incident gamma rays from a source at $x = 0$ cm and without any backscatterer. The integrated intensities of radiation were obtained from the observed pulse-height distribution and by the use of a 20 × 20 inverse response matrix of the NaI(Tl) crystal used in the present work.

In the second part of the experiment the intensity of backscattered radiation was measured as a function of the thickness of the scatterer. Measurements were carried out for gamma rays from a point source in close contact with aluminum and lead scatterers of different thicknesses, with the source position at $x = 0$ cm. The results obtained are shown in Fig. 7. The thickness of the scatterer at which the intensity of backscattered gamma rays incident on the detector become saturated is rather less than that obtained by other workers (*3*, *10*) using parallel or collimated beams.

REFERENCES

1. E. HAYWARD AND J. H. HUBBELL, *J. Appl. Phys.* **25,** 506–509 (1954); *Natl. Bur. Standards (U.S.) Rept.* **2264** (1953).
2. G. J. HINE AND R. C. MCCALL, *Nucleonics* **12,** No. 4, 27–30 (1954).
3. B. P. BULATOV AND E. A. GARUSOV, *J. Nuclear Energy,* Pt. A, *Reactor Science* **11,** 159–164 (1960), [translated from *Atomnaya Energ.* **5,** 631–631 (1958)].
4. R. B. THEUS, L. A. BEACH, AND W. R. FAUST, *J. Appl. Phys.* **26,** 294–297 (1955).
5. N. STARFELT AND H. W. KOCH, *Phys. Rev.* **102,** 1598–1612 (1956); H. W. KOCH AND J. M. WYCKOFF, *IRE Trans. on Nuclear Sci.* **NS-5** 127–137 (1958).
6. T. HYODO AND F. MAKINO, to be published.
7. T. HYODO AND S. SHIMIZU, *Bull. Inst. Chem. Research, Kyoto Univ.* **39,** 180–188 (1961).
8. G. WHITE GRODSTEIN, *Natl. Bur. Standards (U.S.), Circ.* **No. 583** (1957).
9. M. J. BERGER AND D. J. RASO, *Radiation Research* **12,** 20–37 (1960); *Natl. Bur. Standards (U.S.) Rept.* **5982** (1958).
10. M. A. BERGER AND J. DOGGETT, *J. Research Natl. Bur. Standards* **56,** 89–98 (1956).